EMCH 402

Experimental Stress Analysis

Technical Report for Laboratory Exercise 3

Extensometry and Full-Field Deformation Measurements for Experimental Stress Analysis

Author (Lead Author): *Sipos, Emre*

Sections Authored*: Title Page, Introduction, and Theory*

Co-author: *Eden, Jake*

Sections Authored*: Results and Discussion and Summary*

Co-author: *Ankit, Gupta*

Sections Authored*: Materials and Methods*

Writing Team Number: *5*

Tuesday 12:00 – 1:00 pm

Submission Date: *28 April 2024*

Introduction:

In the diverse realm of engineering, analyzing and utilizing materials in different stress and strain environments is crucial for exploring the durability of structures and components. This lab focuses on exploring how multi-scale deformation and in-situ full field analysis methods enable engineers to gather, compare, and analyze contact and non-contact extensometry data of materials such as shape memory alloys (SMA). These methods facilitate data visualization of strain through contour plots, enabling the team to investigate evolving deformation mechanisms and examine the microstructure principles that drive mechanical behavior and material stress-strain response.

This lab experiments with advanced materials in the form of SMAs that display complex deformation mechanics that are not typically exhibited in ductile materials. The specific material used in this lab is a multi-functional Nickel-Titanium alloy (NiTi). This specific alloy is distinguishable by its unique ability to recover from exceptionally high strain rates outside the elastic strain region up to almost 8%. This recovery is facilitated by either adding thermal energy to the SMA which is known as the shape memory effect (SME) or unloading the specimen which is known as the superelastic effect (SE). These unique recovery behaviors are attributed to atomic bond stretching and relaxing during elastic deformation and recovery. Furthermore, the generated strain maps were used to visualize localized strain evolutions throughout all stages of strain evolution.

The lab tested the multi-functional NiTi alloy in two distinguishable methods with both macro-scale and meso-scale analysis. The macro-scale analysis incorporated both non-contact extensometry and contact extensometry. This included the use of an axial non-contact DIC inspect-extensometer driven by the software VIC 2D, alongside a miniature axial contact extensometer (MTS). Alternatively, the meso-scale analysis utilized the data from DIC for a full field analysis in VIC 2D. The resulting data was analyzed by tracking gray-scale subject intensity patterns. These patterns were then mapped by spatially resolving intensity patterns using a Taylor-series expansion.

The main learning objectives for this specific lab were to expose students to multi-scale and in-situ full-field strain analysis using the digital image correlation (DIC) analysis technique. Additionally, the lab aimed to provide practice in experimentally characterizing advanced materials, such as shape memory alloys, that exhibit contrasting deformation mechanics of

typical ductile materials. Additionally, a variety of technical objectives were thoroughly accomplished during the lab session. These included utilizing DIC for quantitative measurements and qualitative analysis of the stress-strain response, conducting uniaxial compression mechanical testing of SMA, and comparing the maximum local strain concentration to the corresponding macroscale stress-strain response. Furthermore, the lab involved performing a qualitative analysis of the deformation mechanics employing in-situ full-field DIC, as well as comparing the morphological evolution of the specimen over time. Moreover, the students reported quantitative measurements of material properties and compared the stress-strain responses from both contact and non-contact methods of extensometry. The exploration extended to understanding extensometry as the science of measurement and analysis of changes in materials linear dimensions during uniaxial testing, along with comparing stress-strain responses determined from measurement and analysis using different gage lengths [7].

Theory:

The theoretical foundation of the experiment conducted is rooted in the underlying principals of extensometry, DIC, strain mapping, and SMAs. Understanding the governing equations of these principals and their constitutive relationships allows further learning regarding the stress-strain techniques. Furthermore, by fundamentally understanding how laboratory procedures operate the student will better learn the assumptions and limitations that led to each method being selected for use in the course.

Extensometry Theory:

An extensometer is defined by the Merriam-Webster dictionary as “an instrument for measuring minute deformations of test specimens caused by tension, compression, bending, or twisting” [1]. They work by having an initial gauge length between two teeth on a specimen that will then allow the extensometer to deform with the specimen as it is exposed to external forces. This essentially allows the extensometer to mimic the specimen while also digitally recording changes in length over time for analysis after the specimen is finished testing. The data that will be recorded by the extensometer is simply a length measurement between the two jaws based on the reference gage length set at the beginning of an experiment seen in figure 1.

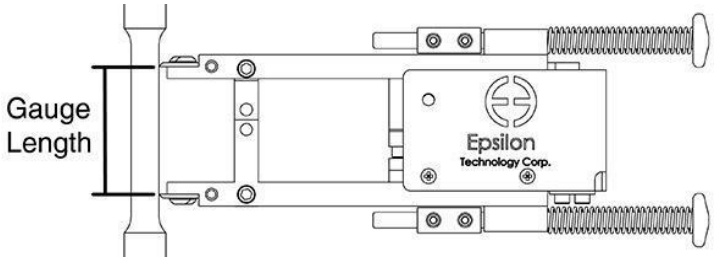

Figure 1. Mechanical Extensometer Configuration [2]

$$_0\varepsilon = \frac{L-L_0}{L_0} = \frac{\delta}{L_0} \quad (1)$$

This length measurement can be processed using the simple strain equation relating the change in specimen length to the original specimen length seen in equation 1. This is considered a macro-scale strain measurement and for our specific experiment yields strain in the y-direction denoted as $\varepsilon_{yy(M)}$. However, installed mechanical strain gages or extensometers come with a certain set of advantages and disadvantages. An extensometer will provide an average strain value over the entire gage length, but is only limited to that gage length. This is important for our experiment because we are dealing with small specimen sizes of roughly 5 mm, but for large scale applications this method would most likely not be the best option. Furthermore, it is in invasive procedure meaning the extensometer will need to be clipped, embedded, or adhered to the tested surface in some capacity which could damage the specimen depending on the material. For this lab, a simple clip will suffice and does not damage the specimen making it an ideal metric of garnering strain measurements over time.

Digital Image Correlation (DIC) Theory:

Digital Image Correlation (DIC) is another method of measuring deformation within a specific gage selection on a specimen. However, DIC operates as a full-field method and does not need physical contact between the specimen and any mechanical part. DIC works by utilizing a painted speckled pattern on the flat surface of a specimen which will deform with specimen over time. As the specimen deforms, images are taken of the speckled surface to see how particles are moving across the surface over time known as strain mapping which will be further discussed later. The most important part of the DIC process is the speckled pattern that is applied to a surface. First, the specimen is painted a solid white base layer coat to give a canvas for the black speckled pattern to be applied. Typically, a light over-misting of black paint with an airbrush

system using fine-tipped attachments is the best technique to yield a balanced speckle pattern. The goal of the pattern is to produce a coating that is not too dense or sparse (figure 2) which will allow the DIC system to take sound resolution pictures of each individual pixel as it shifts over time with deformation. Overall, a non-repetitive isotropic pattern with high contrast makes for the best DIC speckled pattern.

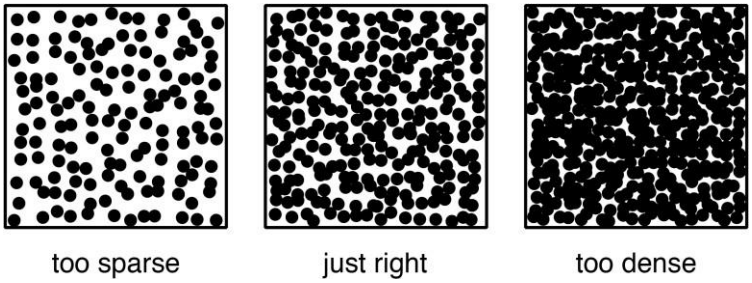

Figure 2. DIC Optimal Coating Visualization [3]

Once painted, an image will be taken of the surface to generate an initial digital image representation. This is done by using computer software on an eight-bit scale of 256 grey levels to assign grey values to each pixel on the coating [9]. The scale starts with a grey value of 0 being black and a grey value of 255 being white. These values are determined by average intensity over the area of the pixel to generate one value for said pixel. This can be better visually understood through appendix figure 23 in grey scale pixel art which follows the same premise. Once each initial pixel is assigned a value, as the specimen is deformed that pixel will be tracked through each subsequent image by this value.

Another critical piece of information regarding DIC is that the camera system typically mounted on a tripod must remain still. For this technique to be effective, the only thing that can be visibly moving during the imaging process is the specimen in front of the camera due to loading. DIC is a sound technique as it does not require contact, it is insensitive to temperature change, and it is full-field method that yields results that are easy to interpret. Furthermore, this technique is much easier to scale up than the previously discussed technique of mechanical extensometer and can be relatively easy to set up in that regard. However, there are a lot of potential drawbacks such as the sensitive speckled pattern which has a meticulous preparation procedure. This speckled pattern must be of the correct density, must be only present on a flat surface, and is sensitive to

light fluctuations. Moreover, DIC requires a direct line of sight from camera to specimen surface and requires the use of VIC-2D for the performing of data correlation.

Strain Mapping Theory:

In the context of DIC, we consider the strain as mapping from a reference configuration to a deformed configuration in a series of images. As discussed, each pixel is assigned a corresponding grey scale value allowing the tracking of that pixel across a surface as specimen transition from a reference configuration to a deformed configuration. These images are then fed into a correction algorithm that calculates the mapping of intensity values and it is assumed that actual surface deformation is described by the same mapping using a Taylor series expansion shown in appendix figure 24. The 2-D DIC code will output x and y directed displacements and displacement gradients. Displacement fields can then be used to calculate strain from the strain displacement relations of normal and shear strain. The assumptions made to make this true is that the speckled pattern adheres and deforms with the surface as well as the fact that homogeneous linear mapping of intensity values maps small reference subsets to the same size deformed subset.

When mapping strain, there are two types of strain to be considered which are normal strain and shear strain than make up the 6 strain-displacement equations. It is important to note that arbitrary points are described by displacement vectors u, v, and w representing the x,y, and z direction. Normal strain is essentially simplified down to the relationship between change in length divided by the original length in the x,y, or z direction seen in equations 2-4 which comprise the first 3 strain displacement equations. As previously discussed, this lab will only deal with 2D mapping meaning that $w = 0$ is a true assumption for these theoretical applications as seen in figure 3.

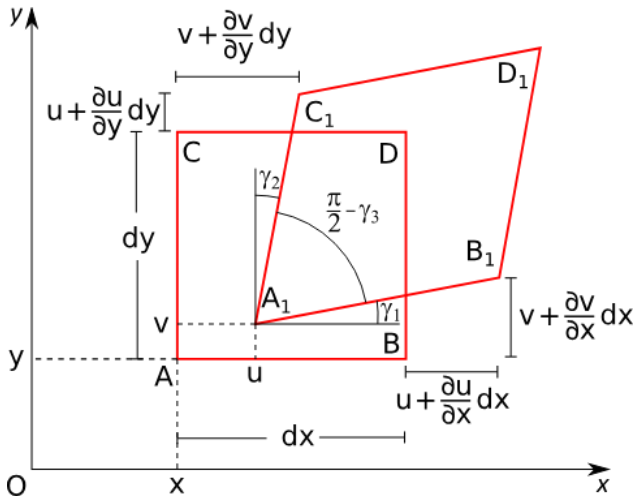

Figure 3. 2-D Strain Displacement Visualization [4]

$$\varepsilon_{xx} = \frac{\partial u}{\partial_x} \text{where } u = u(x,y,z) \tag{2}$$

$$\varepsilon_{yy} = \frac{\partial v}{\partial_y} \text{where } v = u(x,y,z) \tag{3}$$

$$\varepsilon_{zz} = \frac{\partial w}{\partial_z} \text{where } w = u(x,y,z) = 0 \tag{4}$$

Shear strain is essentially the angular change between two originally perpendicular lines. When observing figure 5, the line segments to be compared would be the angular changes from segments AC to A_1C_1 and AB to A_1B_1 which are denoted as γ_2 and c respectively. Thus, wmaking the angle between $C_1A_1B_1$ the measure of $[\frac{\pi}{2} - (\gamma_2 + \gamma_1)]$ as seen in equation 5.

$$\gamma_{xy} = \gamma_1 + \gamma_2 \tag{5}$$

Assuming that the displacements of the materials are to be much smaller than any relevant dimension of the body, small strain theory can be applied which is also known as infinitesimal strain theory. This theory allows small angles to be estimated with the tangential trigonometric operator. For example, in figure 5, the angle $\gamma_1$would be approximated to be equivalent to the expression $\tan\gamma_1$ which can be seen in equations 6 and 7. Plugging these equations back into equation 5 yields a simplified expression for engineering shear strain as seen in equations 8-10. In general, these expressions can be simplified using indicial notation as seen in equation 11 known as the infinitesimal strain tensor that defines the final 3 strain displacement equations.

This simplification is made under the assumptions of small strain as well as that products and squares of displacement gradients are negligible.

$$\gamma_1 \approx \tan(\gamma_1) = \frac{\partial v}{\partial x} \tag{6}$$

$$\gamma_2 \approx \tan(\gamma_2) = \frac{\partial u}{\partial y} \tag{7}$$

$$\gamma_{xy} = \frac{\partial v}{\partial x} + \frac{\partial u}{\partial y} \tag{8}$$

$$\gamma_{xy} = \frac{\partial u}{\partial z} + \frac{\partial w}{\partial x} \tag{9}$$

$$\gamma_{xy} = \frac{\partial w}{\partial y} + \frac{\partial v}{\partial z} \tag{10}$$

$$\varepsilon_{ij} = \frac{1}{2}(u_{i,j} + u_{k,i}) \tag{11}$$

The last step of strain mapping is implementing a subset gray-scale intensity value between undeformed and deformed images. Interpolation functions will help with this by calculating sub-pixel intensities to ensure a unique value corresponds to each portion of the deformed image. These subsets can move, stretch, and even rotate to a deformed configuration. There are a variety of different interpolation functions such as bi-linear, bi-cubic, bi-cubic spline, and quintic spline. These range from the fastest and least accurate being bi-linear to the slowest and most accurate being quintic spline. Navigating these pros and cons is up to the researcher due to the time constraints of research and overall goals of analysis.

Shape Memory Alloy Theory:

As the name suggests, SMAs are capable of returning to their original shape well beyond elastic deformation which is known as super elastic shape memory [8]. This is different from a typical ductile metal elastic to plastic response because a typical ductile material would permanently lose its shape due to plastic deformation as atomic bonds break past the proportional limit for that specific material [5]. A good visualization of this conventional ductile response can be seen in figure 25 of the appendix. This phenomenon must be explored at an atomic structure level to get answers as to why these materials behave in such a manner. At or around room temperature, SMAs exist in their parent or martensite form where the specimen exists in twinned or detwinned martensite form. However, the addition of thermal energy will cause the SMA to undergo a

thermally induced martensitic transformation that will convert the structure into an Austenite crystal structure as seen in figure 4.

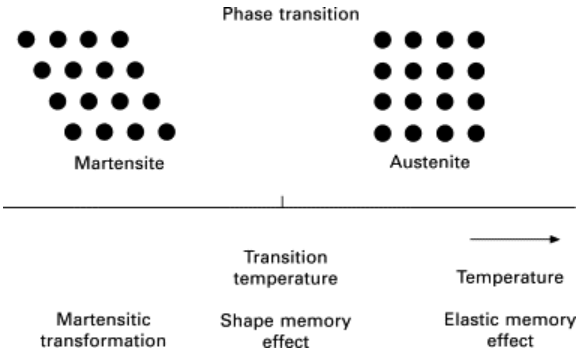

Figure 4. Martensitic Phase Transition Visualization [5]

This is the specific condition for the shape memory effect to transpire, but there is a different effect that needs to be explored as well known as the super elastic effect. In the super elastic effect, external stress induces a martensitic transition which also causes a strain response. However, the strain response is recovered once the external stress is unloaded leading to the original structure to be recovered [6]. These two phenomena make the NiTi SMAs the ideal material to use for this lab as they can be deformed and recovered multiple times for multiple trials. Furthermore, you can also compare the starting images with the final images to gather a true understanding of the capabilities of the SMAs with the shape memory effect.

Materials and Methods:

Material

Nickel-Titanium (NiTi) Shape Memory Alloys (SMAs), shown in Figure 5, are known for their distinctive abilities to remember their original shapes and exhibit super elasticity. These advanced materials were central to the experimental analysis for their capabilities to undergo reversible phase transformations, allowing them to return to their pre-deformed shape upon heating or unloading of stress, an attribute fundamental to their designation as “smart” materials.

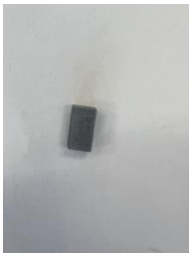

Figure 5. Nickel-Titanium Shape Memory Alloy

The NiTi SMAs used in our experiments were fabricated using conventional wrought processes, as illustrated in Figure 6. This traditional method involves the synthesis of the alloy in a vacuum environment, as highlighted by the Vacuum Arc Melting schematic, Figure 6, which ensures the purity of the material and a homogenous mixture of the Nickel and Titanium components. Following this, the alloy undergoes thermo-mechanical processing, being fashioned into wires, rods, or sheets. This processing stage is crucial as it influences the orientation and size of the grains, which directly impacts the material's mechanical behavior and properties.

The NiTi alloys were subsequently subjected to post-synthesis treatments, such as solution heat treatments and aging, to fine-tune their microstructural characteristics, namely the grain orientation and distribution of microconstituents. This tailoring is critical for ensuring the SMAs perform optimally under specific operational requirements. As the transformation temperatures of these materials are essential to their function, they were meticulously measured using differential scanning calorimetry to confirm their austenitic state during testing, indicative of the material's readiness for stress-induced shape memory transformations.

The specimens were produced as received from the supplier, without any alterations to the material's inherent properties and conditions provided by the manufacturer. The as-received state was crucial to ensure that the results obtained reflected the intrinsic properties of the material, without external modifications influencing the experimental outcomes.

The comprehensive understanding of the behavior of NiTi SMAs under stress was facilitated by the use of extensometer and full-field deformation measurements. These methods allowed for the characterization of the compressive stress-strain response, where the full-field strain analysis illuminated strain contours resulting from localized stress concentrators within the material's microstructure. This in-depth analysis of the meso-scale strain evolution was instrumental in elucidating the complex interactions within the microstructure that drive the mechanical behavior and the properties of SMAs.

The wrought processing of NiTi SMAs is instrumental for applications requiring materials that can withstand intricate stress profiles while maintaining their structural integrity. The precisely tailored microstructures resulting from the thermo-mechanical processes and solution treatments offer a deep understanding of the deformation mechanisms at play. This understanding bridges the gap between the macro scale mechanical responses observable in lab settings and the micro scale interactions that dictate the material's performance in real-world applications. The wrought fabrication of NiTi SMAs for this experimental analysis underscores the importance of precise microstructural control. It ensures that these "intelligent" materials exhibit the desired shape memory and super elastic properties when subjected to the specific demands of advanced applications.

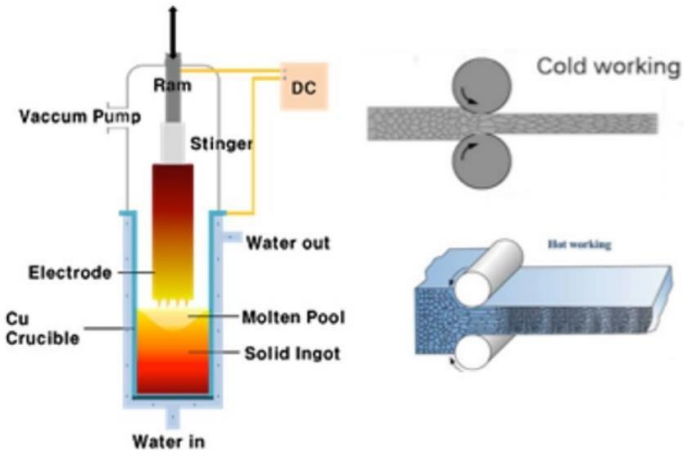

Figure 6. Wrought Process

Experimental Setup and Parameters

The experimental setup for assessing the stress-strain behavior of Nickel-Titanium (NiTi) Shape Memory Alloys (SMAs) combined established and cutting-edge measurement techniques. The key elements included a Servo hydraulic testing system, contact extensometer, and advanced digital image correlation (DIC) for full-field strain analysis.

The centerpiece of the experimental framework was an MTS 810 Material Test System, shown in Figure 7. This system is widely recognized for its precision in exerting and measuring controlled loads, enabling us to determine the mechanical properties of materials with high fidelity. The Servo hydraulic system permitted precise application of compressive loads and captured the macroscopic response of the SMAs to these loads.

Figure 7. MTS 810 Material Test System

For macro-scale strain measurements, a knife-edge clip-type mechanical extensometer was utilized, shown in Figure 8. This device directly attaches to the specimen to measure the deformation over a specific gauge length. These contact measurements were crucial for obtaining reliable strain data at larger scales and for correlating these measurements with microstructural changes in the material.

Figure 8. Contact Extensometer

Speckle patterns, essential for the Digital Image Correlation (DIC) analysis of Shape Memory Alloys (SMAs), are meticulously generated through a controlled painting process. This involves initially coating the SMA surface with a layer of high-flow acrylic paint, shown in Figure 10, to create a uniform, high-contrast background. Once this base layer is dry, a fine mist of carbon black spray paint is applied. The paint nozzle, shown in Figure 9, is held at a sufficient distance,

and moved in a steady, sweeping motion to ensure that the resulting speckles are random in size and distribution. The speckles must be sufficiently dense to enable accurate tracking of surface deformation, yet sparse enough to prevent merging which could confuse the correlation algorithm. The particle size of the spray paint is selected to create sharp edges and high contrast against the white background, which is crucial for the DIC system to detect and follow the speckles during the SMA's deformation. This method results in a high-quality speckle pattern with an optimal distribution that allows for precise strain measurements at both micro and macro scales during experimental analysis.

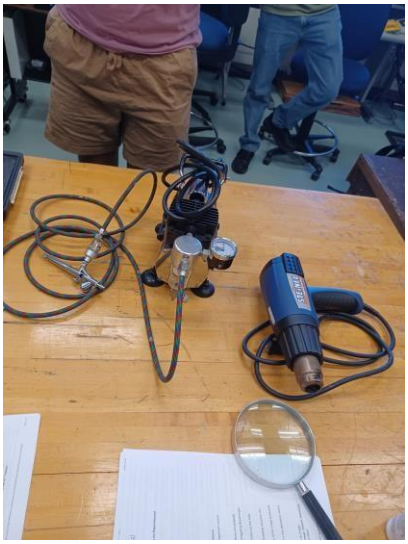

Figure 9. Paint Nozzle

Figure 10. High Flow Acrylic Paint

DIC Analysis with VIC-2D

The Vic-2D system, developed by Correlated Solutions, is a sophisticated optical method for non-contact strain measurement that employs Digital Image Correlation (DIC) technology. This state-of-the-art system is designed to capture and analyze surface deformation by tracking the movement of a speckle pattern applied to the surface of the test specimen.

A key aspect of DIC analysis is the application of a speckle pattern to the specimen's surface. This speckle pattern provides a multitude of unique, identifiable features within the camera's field of view, necessary for accurate tracking through the deformation process.

The Vic-2D system used in our experiment involved a calibrated camera setup, shown in Figure 11, that maintained a specific working distance from the specimen to ensure the entire region of interest was within view. The camera, outfitted with precision lenses, was focused on the speckled surface of the specimen, capturing images before and after deformation.

The DIC technique operates by dividing the captured images into small regions or subsets, each containing several speckles. By tracking the displacement of these subsets between the reference (undeformed) and subsequent (deformed) images, local strains are calculated. The subset size and spacing form a sampling grid over the image, ensuring that sufficient data is collected for detailed strain analysis.

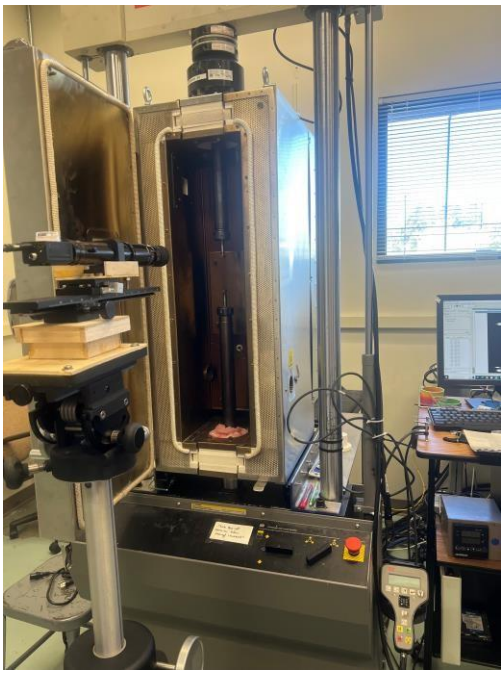

Figure 11. Camera Setup for DIC

Each subset's gray-scale intensity pattern is mathematically mapped from its original to its deformed location, employing robust interpolation functions to calculate sub-pixel intensities. This ensures a high-resolution correlation that can detect and quantify minute surface deformations down to the fraction of a pixel.

VIC-2D, shown in Figure 12, utilizes a correlation coefficient to quantify the similarity between the reference and deformed subsets. By identifying the optimal parameters that minimize the correlation coefficient, the system computes the full-field strain distribution. This iterative process involves an initial guess followed by refinement using algorithms such as the Newton-Raphson method for non-linear optimization. The outcome of this process is a detailed map of strain across the surface of the specimen, providing insights into localized deformation behaviors under stress. The software generates strain contours and displacement vectors, allowing for in-depth analysis of the strain localization and evolution due to the complex deformation mechanisms inherent to SMAs.

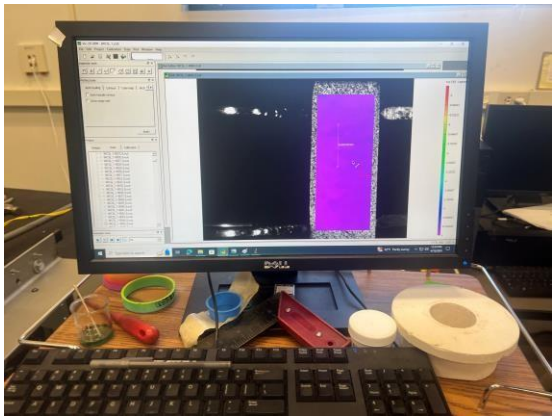

Figure 12. VIC-2D Software

In the experimental setup, Vic-2D played a pivotal role in bridging the gap between macro-scale observations made by traditional extensometers and the intricate, micro-scale behaviors captured through non-contact methods. The detailed strain maps produced by Vic-2D allowed for a comprehensive analysis of the localized effects of stress and strain within the NiTi SMA specimens, providing a deeper understanding of their mechanical responses and underlying deformation mechanisms. The advantages of utilizing the Vic-2D system in experimental stress analysis are manifold. It offers a non-intrusive means to measure strain, avoiding any potential disruption to the specimen's behavior. Moreover, the full-field data provides a richer dataset compared to point measurements, facilitating a more holistic view of material performance under various loading conditions.

Experiment

The experiment was conducted in accordance with ASTM E9 − 19 standards for compression testing. The setup and execution of the experiment followed the recommended procedures for specimen measurement, installation, and alignment to ensure coaxial loading. The system's force and strain measurements were qualified to ensure that the applied loads were axial and uniform, with negligible slip-stick friction.

The experimental procedure was meticulously orchestrated, starting with the precise calibration of the testing system to ensure the accuracy of load and displacement measurements. Calibration involved verifying the alignment and operation of the MTS 810 Material Test System as per the requirements. The NiTi shape memory alloy specimens were carefully mounted within the load frame of the testing system. Attention to detail was crucial at this stage to ensure axial alignment and uniform application of the compressive force, minimizing any potential bending or buckling

that could lead to anomalous data. The setup adhered to ASTM E9 − 19 standard test methods to ensure that the compressive forces were axial, and the setup induced negligible slip-stick friction. Once mounted, the specimens were incrementally loaded in a controlled manner. During the testing process, strain data was continuously recorded using both the mechanical extensometer and the Vic-2D DIC system. The mechanical extensometer, fixed to the specimen, provided direct measurements of macro-scale strain, ensuring high-fidelity data for quantitative analysis. Simultaneously, the DIC system captured a series of images of the specimen surface at each stage of deformation, which facilitated a qualitative assessment of strain distribution.

The data from the mechanical extensometer was critical for capturing the initial linear elastic response and subsequent yield point, providing a clear quantification of the material's mechanical properties. In parallel, the DIC system provided a full-field view of the strain evolution on the specimen's surface, revealing localized deformation patterns, phase transformation zones, and strain concentration areas that are characteristic of SMAs. The simultaneous use of contact and non-contact measurement techniques provided a dual approach to capturing the behavior of the SMAs.

The experimental procedure adopted a rigorous approach to strain measurement that capitalized on the strengths of both traditional mechanical extensometer and advanced optical DIC techniques. This ensured that the stress analysis of NiTi SMAs was both accurate and comprehensive, providing a proper understanding of the material's properties and behavior under stress.

Results and Discussion:

Stress-Strain Curves:

The data collected in this lab was analyzed by turning them into various graphs. Figures 13, as well as 26, 29, and 32 in the appendix, show the stress versus strain relations for the various strain measurement techniques. At first glance, these graphs seem very similar and have the same overall shape. In order to take a deeper dive into the material property values, a new set of graphs were formed and analyzed half the points as the first graph, as seen in figures 14, and 27, 30, and 31 in the appendix. This allowed for a clearer and more focused view of the elastic region of the stress-strain curve. The slope of the line in the elastic region is the elastic modulus. The slope of the line was calculated using the 25^{th} point and the 150^{th} point on each graph using

equation 12. A sample calculation is shown in the appendix. In these same figures, a circle has been placed on the proportional limit. This is where the linear portion of the elastic region ends and gives insight to the stress and strain at this limit. The final critical point for analysis was critical stress. Figures 15, and 28, 31, and 34 in the appendix, show the 0.2% offset line, which was used to find the point of critical stress. All the stress and strain points were collected from each graph and reported using table 1. This table assisted in comparing the material properties calculated from each strain measurement technique.

The biggest outlier from the table was the strain measurements using the actuator. The actuator elastic modulus of 153.77 MPa was six times lower than the highest elastic modulus calculated. Also, the actuator had the highest proportional limit compared to the others. The stress was only 40MPa off the low, while the strain value at the proportional limit was just over seven times higher than the lowest proportional limit. Moreover, while the critical stress value from the 0.2% offset had a stress measurement in line with the other methods, the strain value at this point was over five times larger than the lowest value calculated. This is an expected value as this was the machine is moving and does not directly relate to the strain being experienced in the material. There is more room for error in measurements in this method, as there is no direct analysis or measurement taken from the specimen being tested. The second method was the MTS mechanical extensometer that measured strain over a set distance of the specimen. This method produced results that were significantly closer to the non-contact methods compared to the actuator displacement method. The average elastic modulus for the non-contact method was 975.02 MPa, and the contact method had a percent error of 15.76% compared to this value, which was a significant increase compared to the actuator. Furthermore, there was only a percent error of 6.25% of the stress at the proportional limit, while the difference in the strain value was only 0.1%. The critical stress values were also statistically close as well, as there was only 0.6% difference in the stress value and a difference of 0.1% in the strain values from the 0.2% offset. This method was an improvement as it does measure the strain in the specimen, and not just the movement of the machine. The error in this measurement can stem from the lack of data collected from regions outside of the designated region of the mechanical extensometer.

The final two methods were both non-contact and had very similar results. The elastic modulus of the non-contact method that matches the gage length of the mechanical extensometer only had a percent difference of 0.7% compared to the method using the length of the entire

compression geometry. These methods also had identical values for the proportional limit, which is a significant improvement from the previous two methods. After the 0.2%, the stress values at the critical stress point were identical, while the strain value was measured to be only 0.025% different. These statistics based on the collected data demonstrate the advantages to non-contact methods of measurement and inspection.

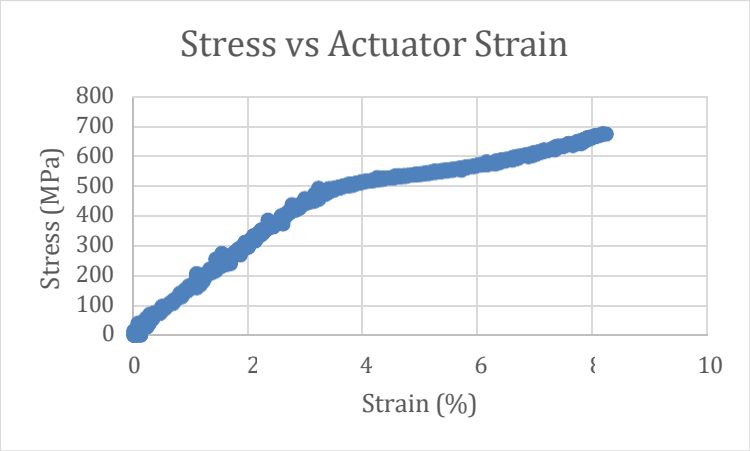

Figure 13. Shows the stress-strain curve from the actuator displacement

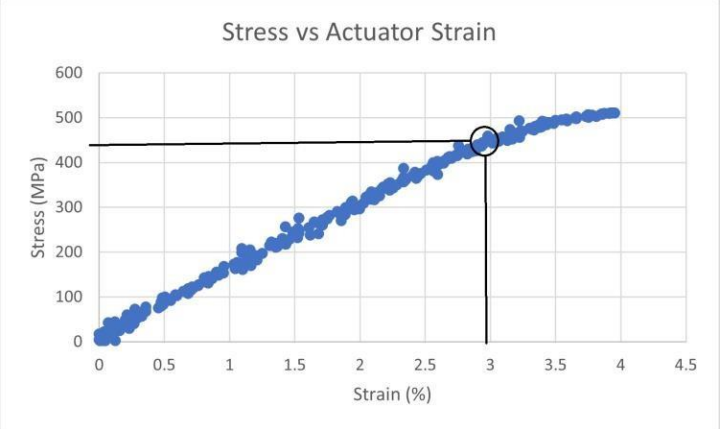

Figure 14. Shows the elastic region of the actuator displacement method with the proportional limit marked.

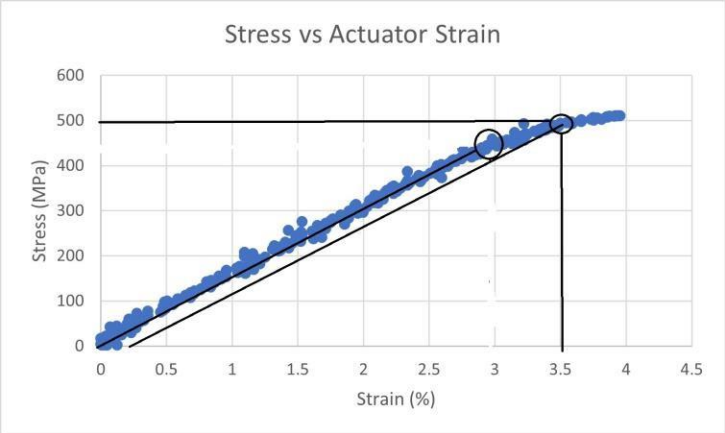

Figure 15. Shows the elastic region of the actuator displacement method with the critical stress point marked.

$$Slope = E = \frac{\Delta y}{\Delta x} \tag{12}$$

Table 1. Tabulated Stress-Strain Results

		Stress-strain response			
		σ_{yy} - $\varepsilon_{yy(act)}$	σ_{yy} - $\varepsilon_{yy(MTS)}$	σ_{yy} - $\varepsilon_{yy(M)}$	σ_{yy} - $\varepsilon_{yy(h)}$
Modulus	E(*)	153.77 MPA	821.37 MPA	971.53 MPA	978.50 MPA
Proportional limit (corresponding stress and strain)	σ_{pl} (*)	440 MPA	425 MPA	400 MPA	400 MPA
	ε_{pl} (*)	2.95%	0.5%	0.4%	0.4%
Critical Stress (0.2 % offset corresponding stress and strain)	σ_{cr} (*)	500 MPA	498 MPA	495 MPA	495 MPA
	ε_{cr} (*)	3.5%	0.75%	0.65%	0.675%

Poisons' Ratio:

While the stress-strain curves gave insight to the difference in various material properties, further analysis needed to be done to analyze poison's ratio. To effectively find the Poisson's'

ratio, two graphs were created to create a relationship between the axial and transverse strains in the non-contact methods. Figure 16 shows the relationship between axial and transverse strain of the non-contact method with a distance set to the same as the mechanical extensometer. Figure 17 shows the same relationship, but with the data collected by changing the distance to the entire compression geometry. These graphs were very similar, which was expected due to the similar results in the stress-strain curves. The Poisson's ratio was calculated through finding the slope of the line. This is explained through equation #. Since the Poisson's ratio is axial strain/transverse strain, the slope is the same relationship and can therefore create a value for this ratio. Equation # was used again for this calculation. The 25th and 150th points on each graph were used once again for calculations. A sample calculation can be found below in the appendix. Table 2 shows the results after calculations.

$$\nu = -\frac{s_{yy}}{s_{xx}} \tag{13}$$

Table 2. Tabulated Poisson's Ratio Results

Poisson's Ratio of specified region in non-contact method	-2.082
Poisson's Ratio of entire compressed geometry in non-contact method	-2.067

As stated before these values were very similar as there was only a 0.73% difference between values. This shows the consistency of the non-contact method and how inspecting using this method can decrease error.

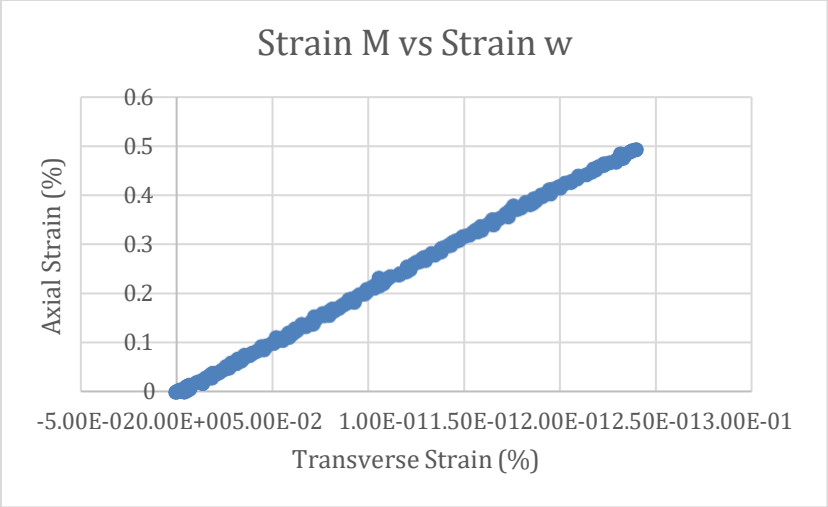

Figure 16. Shows the relationship between axial and transverse stress in the specified region.

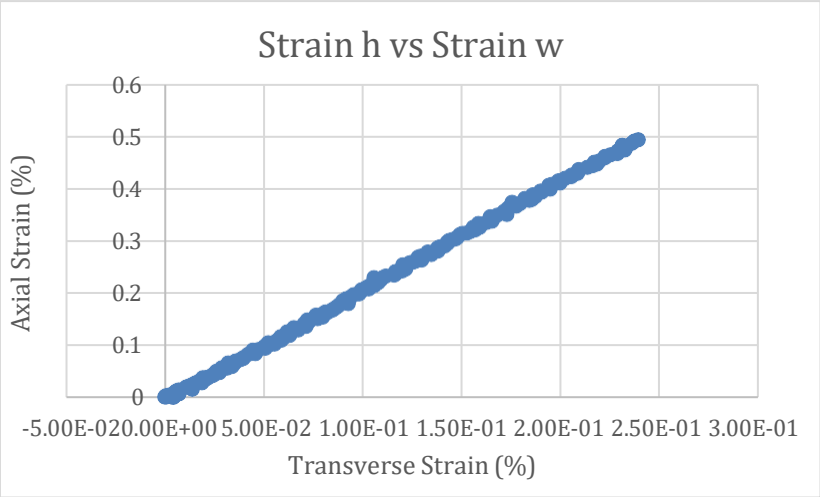

Figure 17. Shows the relationship between axial and transverse stress over the entire length of the geometry.

Meso-Scale Strain:

In addition to traditional strain measurements, DIC methods can give additional information to the strain breakdown in the geometry of the specimen. In figure 18, the baseline of the strain is shown. Here there is 0% strain and is one solid color. This baseline helps to compare changes over the course of the applied stress. Next, figure 19, shows the new strain concentration at the proportional limit. Here there is a max strain of approximately 0.5%.

The concentration scale can be referenced below in the appendix. It is also clear that the overall deformation concentration has changed from the original. There are only splotches of pink throughout the geometry. There demonstrates how the progression of strain is not constant and does not impact every area of the geometry the same. Thirdly, figure 20, shows the concentration at the critical stress point. Here, the max strain is approximately 0.65%. Furthermore, the concentration at this point is mainly solid blue, which progressed from the mix of purple and pink seen at the proportional limit. In this image there are still remains of pink at the bottom of the geometry. There are also faint hints of pink on the right edge of the specimen as well, indicating the majority of the concentration of the strain is focused on the center of the specimen. Moreover, figure 21 highlights the concentration as the stress-strain relationship progresses more into the plastic region. In this image you can still see some pink in the bottom right corner indicating that strain has not occurred in that region yet. There is also green in the upper two thirds of the specimen, with yellow in the upper left corner, indicating an increased level of strain. There is still blue present in the lower regions, but it is beginning to break up and not be solid as it was at the point of critical stress. The max stress experienced in this image is approximately 2.75%. Finally, figure 22 shows the strain concentration at the peak load. This image shows the biggest change from all of the others. At the max load, there is no longer pink present in the specimen, so every part of the specimen has experienced strain. There is still some blue in the lower right corner of the specimen, but the upper two thirds turned to a mix of orange and yellow indicating the highest level of strain. The lower third also progressed from blue to green as strain increased. The max strain present at this point was approximately 4.5%.

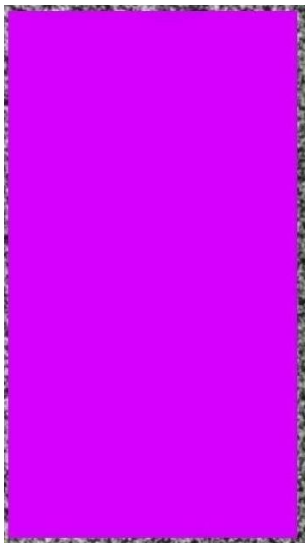

Figure 18. Shows the strain concentration before additional loading.

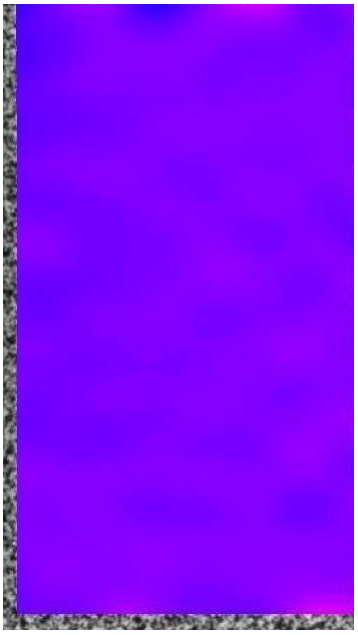

Figure 19. Shows the strain concentration at the proportional limit.

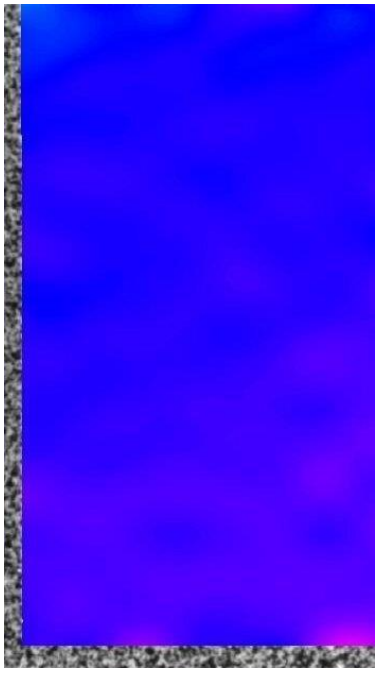

Figure 20. Shows the strain concentration at the critical stress point

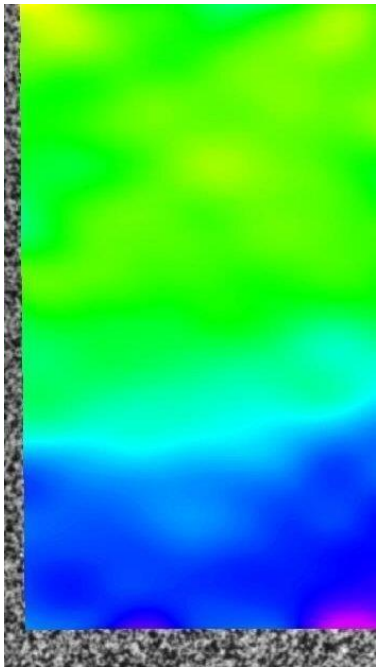

Figure 21. Shows the strain concentration deeper into the plastic region.

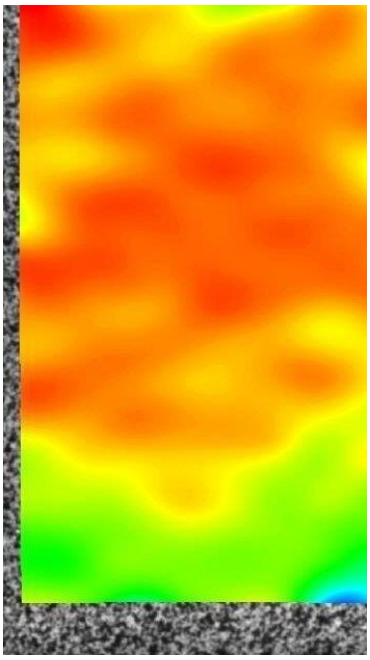

Figure 22. Shows the strain concentration at the max load.

Summary:

Overall, this lab provided great insight into the advantages of DIC methods for stress-strain analysis. While contact methods can give great insight to material properties and how a specimen reacts under stress, it became clear that it can not provide a full analysis like DIC methods are capable of. This was seen in the increased accuracy of the stress-strain curves as well as key points such as the proportional limit and critical stress value. These values saw a significant decrease in percent error when DIC methods were applied. Furthermore, the meso-scale images allow for even deeper analysis. Strain does not occur evenly across the entire geometry, and some areas may experience significantly elevated levels of stress compared to other regions. This becomes critical information in evaluating a design or specimen to see where failure may occur, or the specimen could become weak over time. The information that DIC methods provide is invaluable to engineering and testing safe designs in the future. While there is and always will be a place for contact methods of analysis, DIC is another tool to dive deeper into what is truly occurring throughout the geometry of the specimen. With any method there is room for error, and one blurry image or a different angle could skew data, but as a whole, DIC methods can be very accurate and helpful in stress-strain analysis. In future experiments non-contact methods of

analysis can and will be used more for deeper understanding of the response within the specimen.

References:

[1] Merriam-Webster. (n.d.). *Extensometer definition & meaning*. Merriam-Webster. https://www.merriam-webster.com/dictionary/extensometer

[2] *Extensometer Basics*. Epsilon Tech. (2023, June 20). https://www.epsilontech.com/extensometer-basics/#:~:text=Extensometers%20measure%20the%20extension%2C%20compression,by%20its%20original%20gauge%20length.

[3] *Digitalimagecorrelation.org*. digitalimagecorrelation.org. (n.d.). https://digitalimagecorrelation.org/

[4] *File:strain-displacement-2d.SVG*. Wikimedia Commons. (n.d.). https://commons.wikimedia.org/wiki/File:Strain-displacement-2D.svg

[5] *Martensitic transformation*. Martensitic Transformation - an overview | ScienceDirect Topics. (n.d.). https://www.sciencedirect.com/topics/chemistry/martensitic-transformation

[6] *Superelasticity*. Superelasticity - an overview | ScienceDirect Topics. (n.d.). https://www.sciencedirect.com/topics/materials-science/superelasticity#:~:text=Superelasticity%20occurs%20when%20an%20external,in%20NiTi%20shape%20memory%20alloys.

[7] *R. Hamilton. "SP24 Lab 3 Overview" Pennsylvania State University (2024) https://psu.instructure.com/courses/2310697/pages/sp24-lab-3-overview?module_item_id=41493471*

[8] *R. Hamilton. "SP24 Lab 3 Materials Background" Pennsylvania State University (2024) https://psu.instructure.com/courses/2310697/pages/sp24-lab-3-materials-background?module_item_id=41493472=41493471*

[9] *R. Hamilton. "SP24 Lab 3 Test Specimen and Target Pattern Details" Pennsylvania State University (2024) https://psu.instructure.com/courses/2310697/pages/sp24-lab-3-test-specimen-and-target-pattern-details?module_item_id=41493645*

[10] *R. Hamilton. "SP24 Lab 3 Deformation Measurements and Strain Analysis" Pennsylvania State University (2024)* https://psu.instructure.com/courses/2310697/pages/sp24-lab-3-deformation-measurements-and-strain-analysis?module_item_id=41493646

[11] *R. Hamilton. "SP24 Lab 3 Thermo-mechanical Experimentation"Pennsylvania State University (2024)* https://psu.instructure.com/courses/2310697/pages/sp24-lab-3-thermo-mechanical-experimentation?module_item_id=41494033

[12] kamal_DS. (2023, January 24). *Gray scale and color images using opencv*. Medium. https://korlakuntasaikamal10.medium.com/gray-scale-and-color-images-using-opencv-eda0c13c292a

[13] *AI-Powered Research Tool*. Semantic Scholar. (n.d.). https://www.semanticscholar.org/

Appendix:

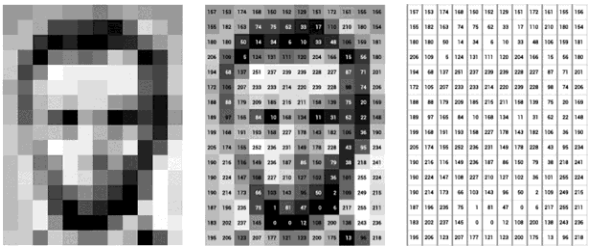

Figure 23. Grey Scale Example of 8-bit Pixel Art [12]

Assume uniform strain inside a subset (homogenous linear mapping)

$$x^* = x_0 + u_0 + \frac{\partial u}{\partial x}\Delta x + \frac{\partial u}{\partial y}\Delta y + \cancel{\frac{1}{2}\frac{\partial^2 u}{\partial x^2}\Delta x^2} + \cancel{\frac{1}{2}\frac{\partial^2 u}{\partial y^2}\Delta y^2} + \cancel{\frac{\partial^2 u}{\partial x \partial y}\Delta x \Delta y}$$

$$y^* = y_0 + v_0 + \frac{\partial v}{\partial x}\Delta x + \frac{\partial v}{\partial y}\Delta y + \cancel{\frac{1}{2}\frac{\partial^2 v}{\partial x^2}\Delta x^2} + \cancel{\frac{1}{2}\frac{\partial^2 v}{\partial y^2}\Delta y^2} + \cancel{\frac{\partial^2 v}{\partial x \partial y}\Delta x \Delta y}$$

Figure 24. Taylor Series Expansion for Homogeneous Linear Mapping

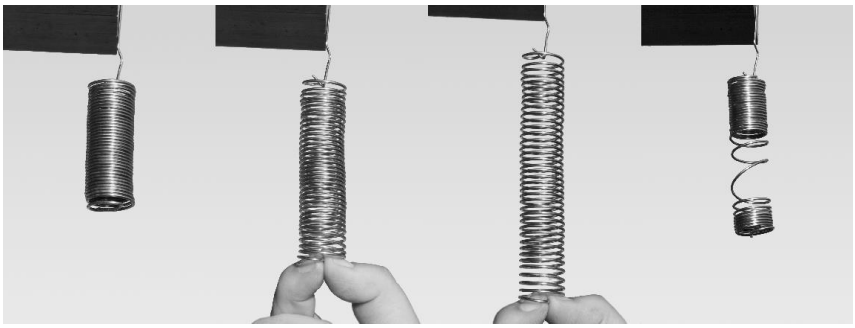

Figure 25. Normal Ductile Material Plastic Deformation [13]

Sample Calculation: Stress-Strain for MTS

$$Slope = E = \frac{(350.2383 - 40.58209)}{(0..3996 - 0.0226)} = 821.369\ MPa$$

*S*ample Calculation: Poisson's Ratio M vs W

$$slope = \nu = -\frac{\Delta y}{\Delta x} = -\frac{s_{yy}}{s_{xx}} \quad \frac{(0.34019-0.02146)}{(0.165337-0.012285))} = -2.082$$

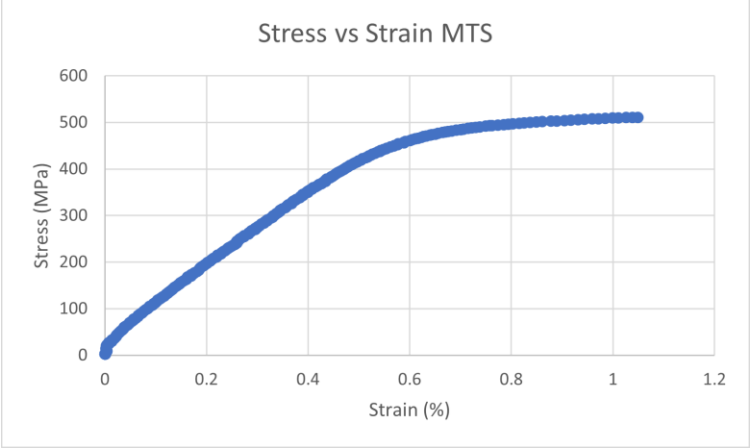

Figure 26. Shows the stress-strain curve of the MTS method.

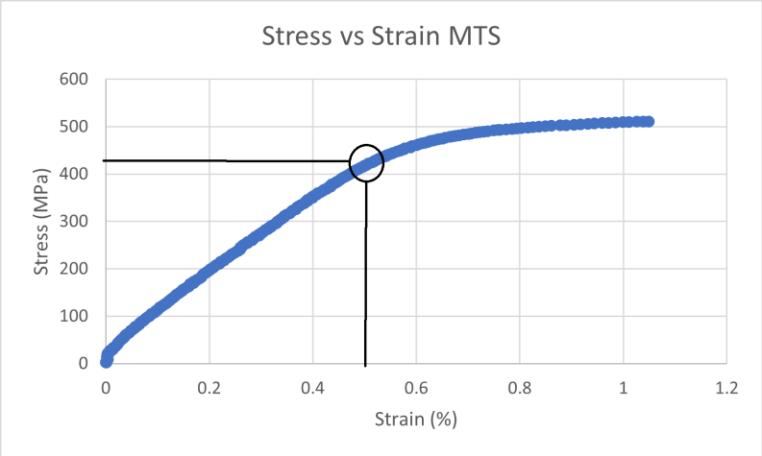

Figure 27. Shows the proportional limit of the MTS method.

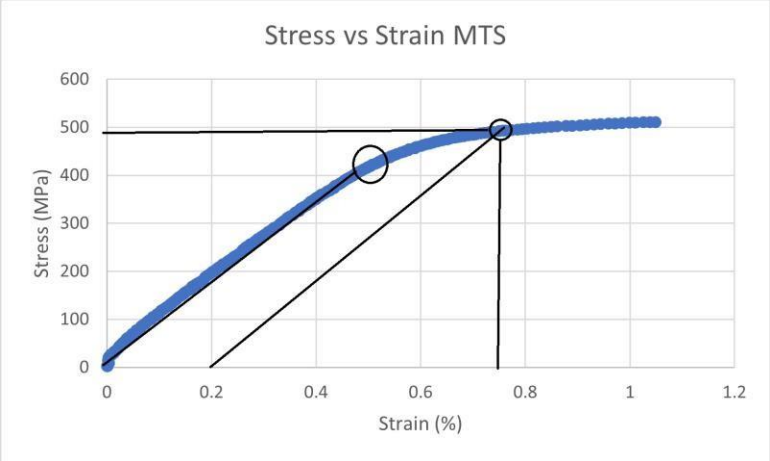

Figure 28. Shows the critical stress point of the MTS method.

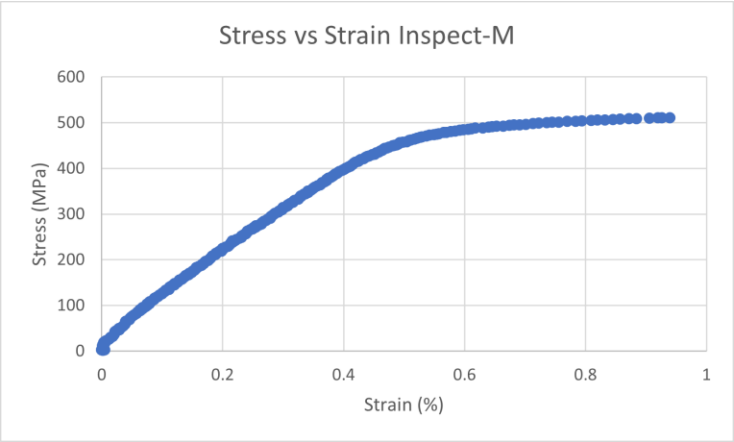

Figure 29. Shows the stress-strain curve of the non-contact method with a set measurement distance.

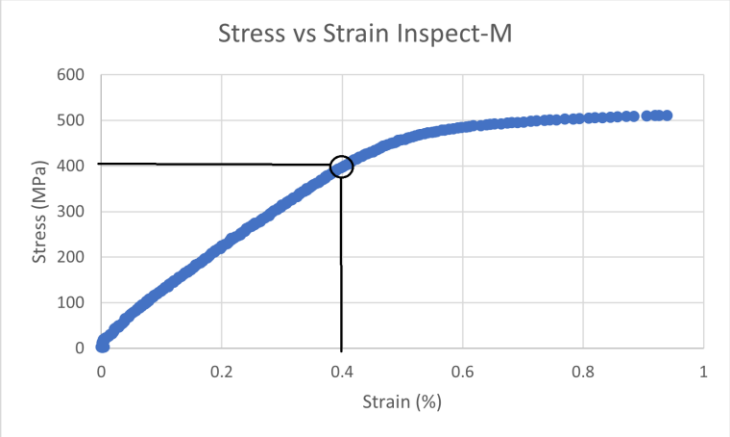

Figure 30. Shows the proportional limit of the non-contact method with a set measurement distance.

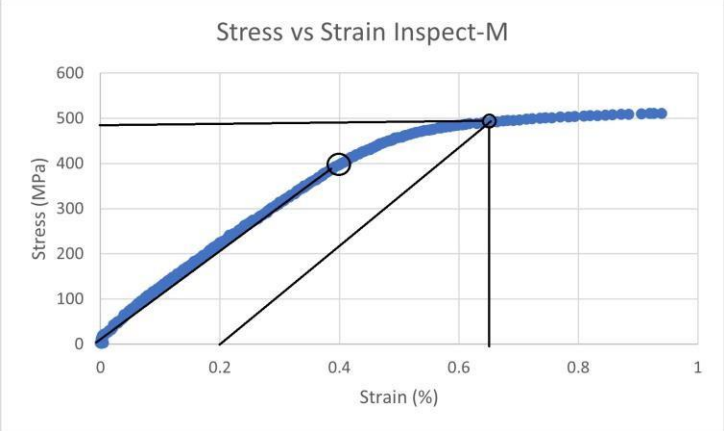

Figure 31. Shows the critical stress point of the non-contact method with a set measurement distance.

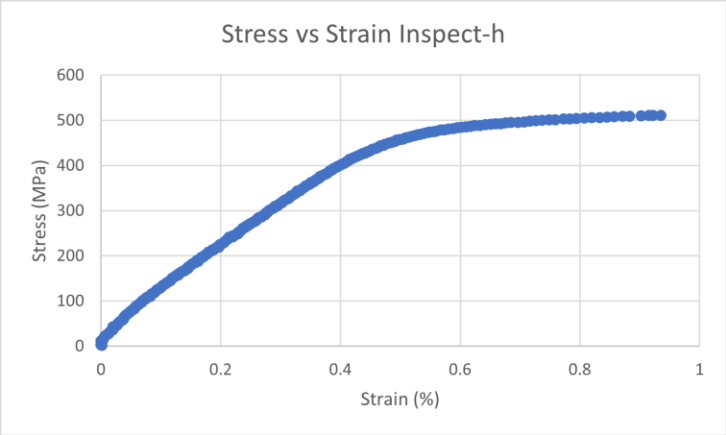

Figure 32. Shows the proportional limit of the non-contact method over the entire compression geometry.

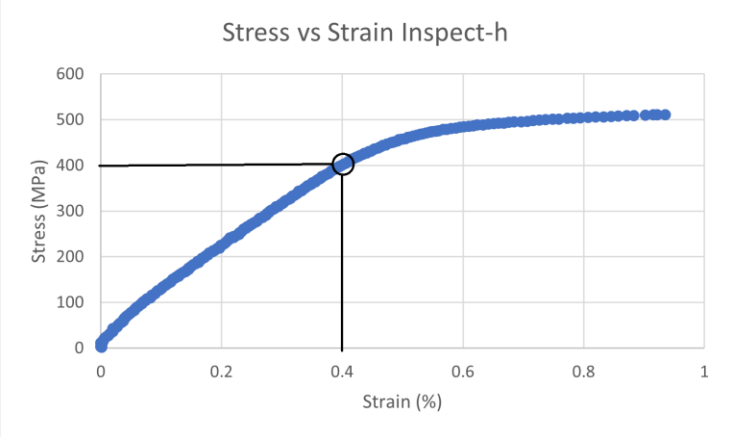

Figure 33. Shows the proportional limit of the non-contact method over the entire compression geometry.

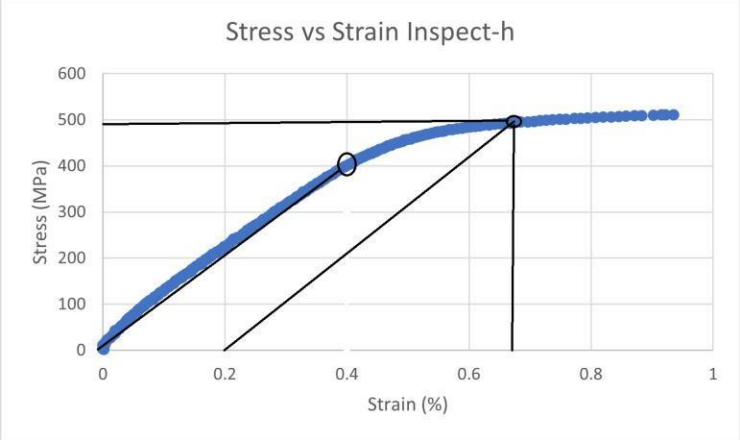

Figure 34. Shows the critical stress point of the non-contact method over the entire geometry.

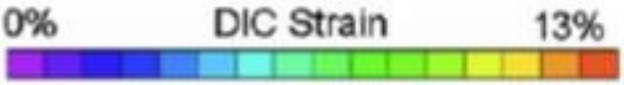

Figure 35. Shows the strain concentration scale.